11-10-2000

Continuum Pumping of [Fe II] in the Orion Nebula

E. M. Verner
University of Kentucky

D. A. Verner
University of Kentucky

J. A. Baldwin
National Optical Astronomy Observatoires, Chile

Gary J. Ferland
University of Kentucky, gary@uky.edu

P. G. Martin
University of Toronto, Canada

Continuum Pumping of [Fe II] in the Orion Nebula

Notes/Citation Information
Published in *The Astrophysical Journal*, v. 543, no. 2, p. 831-839.

Digital Object Identifier (DOI)
http://dx.doi.org/10.1086/317159

THE ASTROPHYSICAL JOURNAL, 543:831–839, 2000 November 10

CONTINUUM PUMPING OF [Fe II] IN THE ORION NEBULA

E. M. VERNER,[1,2] D. A. VERNER, [1] J. A. BALDWIN,[3] G. J. FERLAND,[1] AND P. G. MARTIN[2]

Received 2000 May 11; accepted 2000 June 20

ABSTRACT

This paper presents detailed comparisons between numerical simulations of Fe II emission spectra and recent high-resolution and signal-to-noise spectra of the Orion Nebula. We have identified 40 [Fe II] lines in the spectrum, allowing extensive comparisons between theory and observations. The identifications are based on predictions of a realistic model of the Fe II atom, which includes the lowest 371 levels (all levels up to 11.6 eV). We investigate the dependence of the spectrum on electron density and on pumping by the stellar continuum. Orion is important because it provides a relatively simple environment in which to test complex simulations. We have identified the pumping routes that are responsible for the observed emission. Our theoretical model of Fe II emission is in good agreement with the observational data.

Subject headings: atomic data — H II regions — ISM: individual (Orion Nebula) — line: formation — line: identification

1. INTRODUCTION

Fe II emission from regions of ionized gas is ubiquitous. Under some conditions (such as in active galactic nucleii), Fe II can be a major factor in the energy balance of the gas, and even when it is not, the great number of Fe II lines must be carrying considerable information about the physical conditions in the gas. Therefore, developing diagnostics based on [Fe II] line ratios is a very active field of research. The aim is to obtain consistent models of the velocity field, density, excitation conditions, and abundances. There are considerable uncertainties in the atomic data and the physical processes are complex, so it is necessary first to validate spectral indicators by comparisons in relatively simple environments. H II regions are good laboratories for this purpose since Fe II does not dominate the physics, and enough information is available from other diagnostics to fully constrain a model.

Studies of [Fe II] lines observed in the Orion Nebula have shown that some intensities ratios *cannot* be explained by pure collisional excitation at the densities $n_e \sim 10^4$ cm^{-3} deduced from nitrogen and oxygen forbidden lines. Bautista, Pradhan, & Osterbrock (1994) postulated the existence of high-density partially ionized regions with $n_e \sim 10^6$ cm^{-3} in order to explain these discrepancies. Esteban et al. (1998) and Baldwin et al. (2000) presented reliable detections of the [O I] λ5577 line in the Orion Nebula and, in two different independent ways, confirmed that the [O I] and [Fe II] lines are indeed formed in lower density gas. How then are the [Fe II] lines discussed by Bautista et al. excited?

Lucy (1995) has shown that some anomalously strong [Ni II] lines can be explained by fluorescent excitation of Ni^+ levels by the UV stellar radiation. In fact, some Fe II lines may be predominantly excited by the stellar continuum (Baldwin et al. 1996). Recently, Rodriguez (1999) showed that the intensities of [Fe II] lines in different H II regions are strongly correlated with the intensity of the diffuse continuum, further strengthening the case that some lines are radiatively rather than collisionally excited. Meanwhile, Baldwin et al. (2000) identified 40 [Fe II] emission lines, double the previous number of known [Fe II] lines (Esteban et al. 1998) in the 3498–7468 Å range. This extensive data set gives us a new chance to identify the excitation mechanisms.

The main goal of this paper is to create a complete numerical model of the Fe II atom as part of fully self-consistent photoionization calculations. Our Fe II model atom is described by Verner et al. (1999), while Baldwin et al. (1996) outlines our previous work on [Fe II] and physical conditions in the Orion Nebula.

In § 2, we investigate the sensitivity of the populations of all levels to continuum pumping, and the sensitivity of Fe II emission to electron density, for conditions similar to the Orion Nebula. We show that some levels are very sensitive to pumping and therefore cannot be used for density diagnostics. We also investigate the general behavior of Fe II emission lines over the UV through optical and infrared wavelengths. In § 3, we model the spectrum of the Orion Nebula using the new observations presented by Baldwin et al. (2000). We present detailed comparisons between the observed and predicted lines.

2. THE PREDICTED [Fe II] SPECTRUM

2.1. Fe II *Atom Model*

Our current model of the Fe II atom includes all 371 levels with energies below 93487.650 cm^{-1}, or 11.59 eV. All level energies are experimental (Johansson 1978) and should be quite accurate. Throughout this paper, we will refer to the level numbers, which are obtained by ordering the Fe II levels by energy from 0 (level 1) to 93487.65 cm^{-1} (level 371; see Johansson 1978, Tables V and VI). Our sources of radiative and collisional atomic data are described by Verner et al. (1999). Our current model includes updates to collisional strengths for transitions between the lowest 63 levels (M. Bautista, 1999, private communication).

The Fe II model atom has been added into the radiative-collisional code CLOUDY (Ferland et al. 1998). The basic equations of ionization and thermal balance, level popu-

[1] Department of Physics and Astronomy, University of Kentucky, Lexington, KY 40506-0055; gary@pop.uky.edu.

[2] Department of Astronomy, and Canadian Institute for Theoretical Astrophysics, University of Toronto, Toronto, ON, Canada M5S 3H8.

[3] Cerro Tololo Inter-American Observatory, National Optical Astronomy Observatories, Casilla 603, La Serena, Chile. NOAO is operated by AURA, Inc. under contract to the National Science Foundation.

lations, and radiative transfer are solved self-consistently. The Fe II level populations are obtained numerically by solving the set of balance equations. The final solution is obtained by iteration, with the feedback effects of Fe II emission on the radiative and thermal environment explicitly taken into account.

2.2. *Level Population Sensitivity to the Pumping Conditions*

Forbidden oxygen and nitrogen lines, e.g., [O II] λ3727 or [N II] λ6584, are collisionally excited in H II regions and can be used for density diagnostics (Osterbrock 1989). The observed [Fe II] optical lines have similar excitation and ionization energies. However, the structure of the Fe II atom is much more complicated. Noncollisional excitation mechanisms, including pumping of high Fe II levels by the UV stellar continuum and subsequent downward cascades, can contribute significantly to the observed intensities of the optical [Fe II] lines. To determine which [Fe II] lines can be used for density diagnostics, it is first necessary to find which levels are more affected by pumping than by collisions. We do this by investigating the behavior of the level populations for conditions appropriate to H II regions (Baldwin et al. 1996; Verner et al. 1999).

First, we did simple one-zone (optically thin) calculations assuming conditions similar to the Orion Nebula: $n_e = 10^3$ cm^{-3}, a depleted iron abundance, and nebular abundances for all other elements (Baldwin et al. 1996). We intentionally chose a low density, which minimizes collisional effects, to determine which lines are nevertheless mainly excited by collisions.

In our first calculation, we included continuum pumping by blackbody radiation with temperature 35,000 K and ionization parameter $U = \Phi_H/n_H c = 10^{-3}$, where Φ_H is a flux of hydrogen ionizing photons, n_H is the hydrogen nucleon density, and c is the speed of light. This radiation field is close to that in the Orion Nebula. We then repeated the calculation but without any pumping processes. Finally, the ratio of level populations for these two cases was calculated. Elevation of this ratio above unity indicates a sensitivity of that level's population to continuum pumping.

In Figure 1*a*, the x-axis shows the number of the level in the atom, and the y-axis shows the logarithm of the level population ratios. The levels that have a small change can be considered as upper levels for lines that will not be very sensitive to pumping. If a level population changes by 20% or higher because of radiative pumping, then lines from the affected levels are not appropriate to use for accurate density diagnostics. Our calculations show that only the very lowest levels (16 levels in four multiplets) are sufficiently collisionally dominated that they can be a reliable basis for density diagnostics for all conditions. These levels can be considered as collisionally excited. Transitions "safe" for density diagnostics are marked with numbers 12 ($\lambda\lambda$8616.96, 8891.88), 13 (λ12567), and 14 (λ16435) on Figure 3.

Higher energy levels become harder and harder to excite by collisions at a given temperature. By comparison, contin-

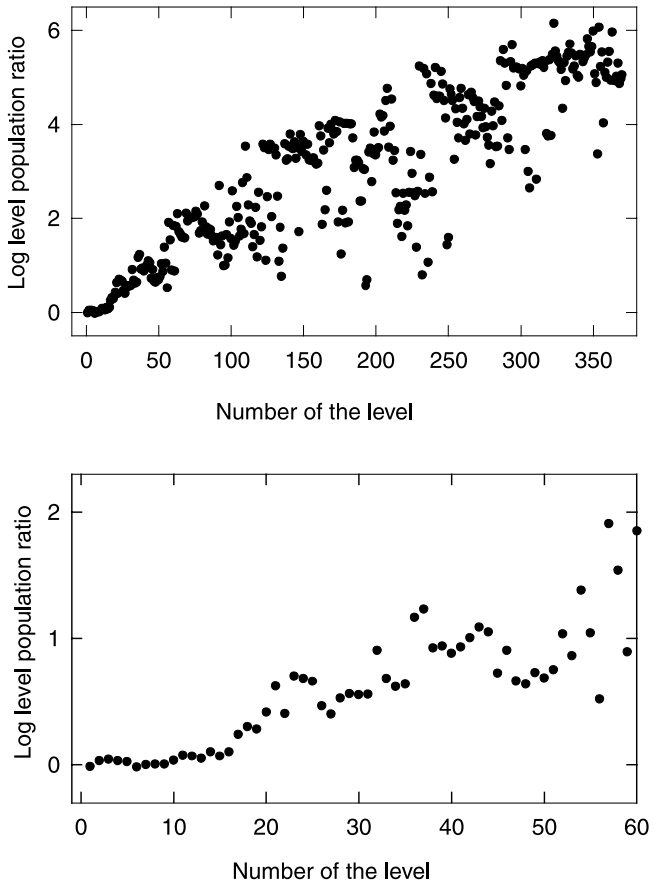

FIG. 1*a*

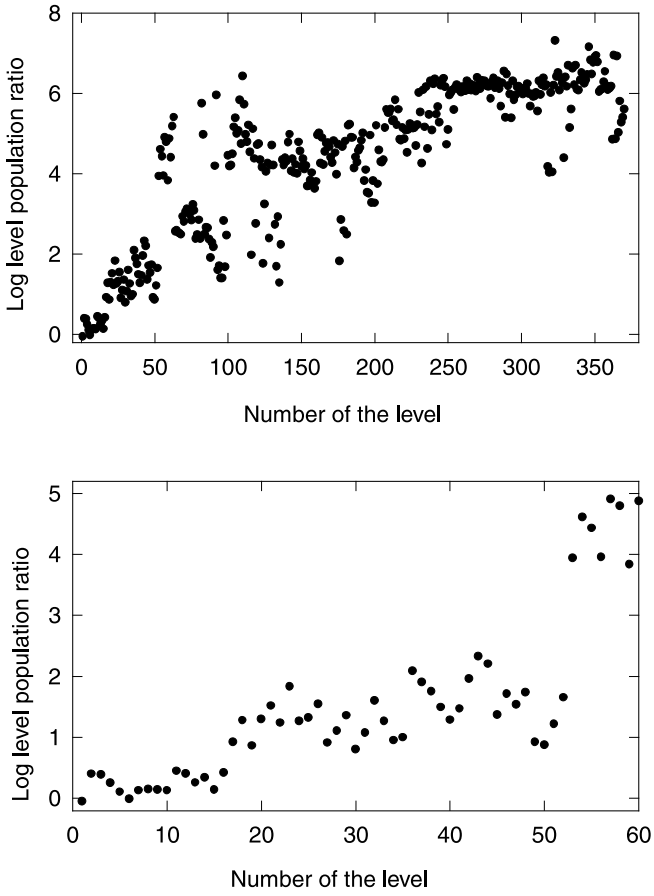

FIG. 1*b*

FIG. 1.—(*a*) Log of the Fe II level population ratio (with/without pumping) for one-zone calculations under conditions similar to the Orion Nebula with blackbody 35,000 K continuum. (*b*) Same as (*a*) but with continuum from all four Trapezium stars.

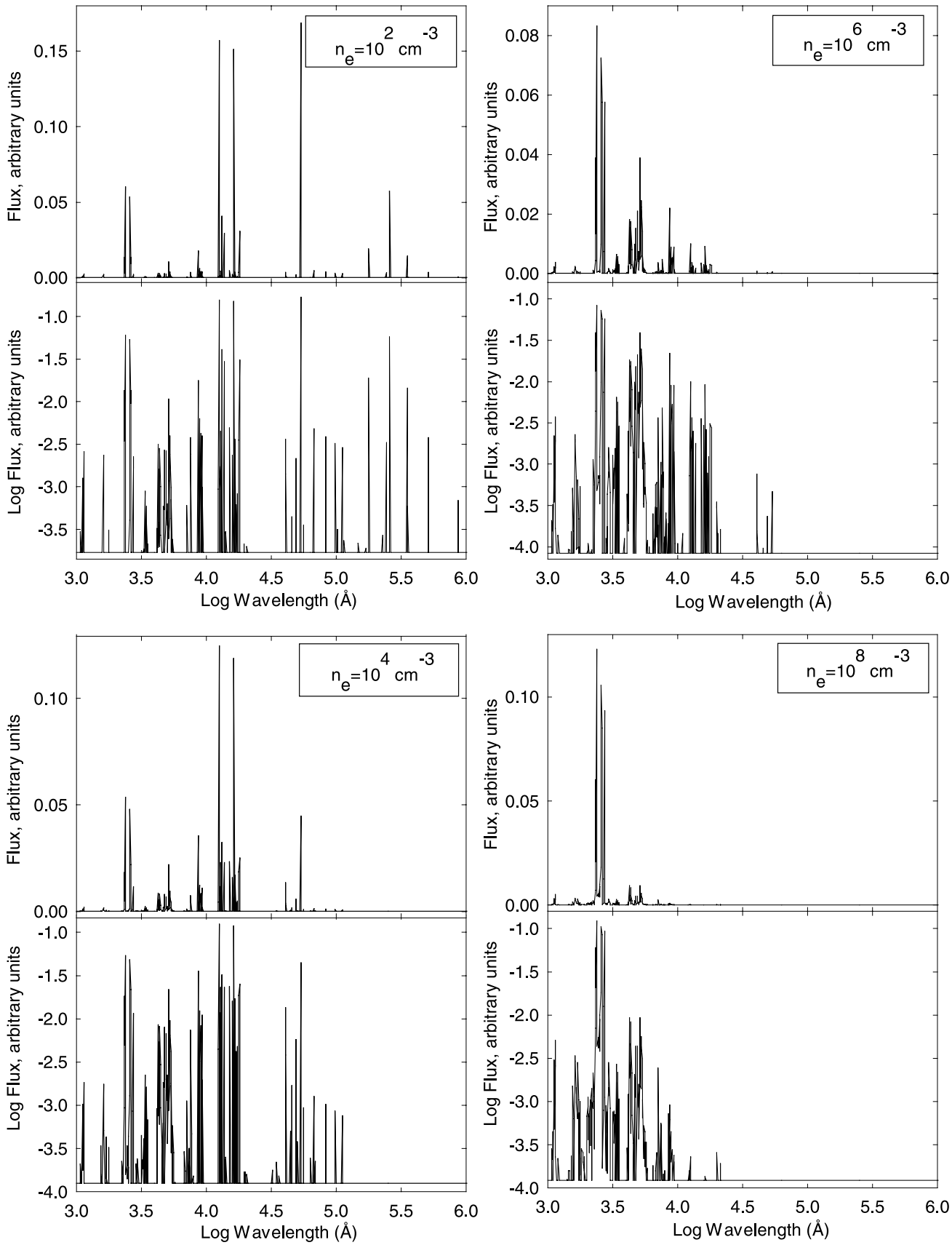

FIG. 2.—Fe II emission-line fluxes (normalized and binned, at resolution $\cong \lambda/\lambda = 3 \times 10^{-3}$) for one-zone calculations with conditions similar to the Orion Nebula and densities 10^2, 10^4, 10^6, and 10^8 cm^{-3}. At each density, the upper panel is on a linear scale to show all lines and the lower panel is on a logarithmic scale.

uum pumping has no direct temperature dependence. This is why pumping is relatively more important for the higher levels (this is the trend upward to the right in Fig. 1*a*). Nevertheless, even though these pumped levels are 10^6 times overpopulated by pumping, relative to the non-pumped case, they have very low populations (because of the small Boltzmann factors) and so do not produce strong lines.

Figure 1*b* shows the same Fe II level population ratio as Figure 1*a* but includes the effects of all four Trapezium stars (an estimated 70% of the total flux at 2300 Å is caused by θ^1 Ori C). A comparison between Figure 1*a* and Figure 1*b* shows the enhanced importance of continuum pumping. In this case, even the lowest 16 levels' populations are influenced by pumping at the density $n_{\rm H} = 10^3$ cm^{-3}.

However, we found in more realistic many-zone models including the effects of opacity that the lowest 16 levels can safely be used as density diagnostics. The illustrative one-zone calculations tend to overestimate the radiative pumping since the radiation field is unattenuated and so somewhat overestimates the importance of pumping relative to collisions compared with the actual (more realistic) Orion Nebula model described below. Furthermore, collisions are underestimated here since we chose a density of $n_{\rm H} = 10^3$ cm^{-3} compared with the actual density of $n_{\rm H} = 10^4$ cm^{-3} in the innermost regions of the Orion Nebula. Some of the levels shown as sensitive to pumping might actually be collisionally dominated in some situations. In the Orion Nebula models below, neither λ8617 (often used as a normalizing line; from level 14) nor λ8892 (from level 15) is affected by pumping.

2.3. *The Sensitivity of* Fe II *Emission to Electron Density*

To assess the effects of density on the Fe II emission, we repeated the general one-zone calculations for the density range 10^2–10^8 cm^{-3}. The ionizing flux and chemical abundances were the same as in the model described above. To show the results graphically, we first integrated the total Fe II emission over all wavelengths (to use as a normalizing value), then divided the whole range into about 10^3 cells with resolution 3×10^{-3}. Figure 2 shows the line fluxes relative to the total emission, with the upper panels on a logarithmic scale (to show faint lines), and the lower panels on a linear scale.

The spectrum is very rich throughout the entire wavelength range at low densities, $\sim 10^2$–10^4 cm^{-3}. The forbidden near-infrared and far-infrared lines are the strongest, and the permitted optical lines are relatively weak. The reason is that the 63 lowest levels, the most populated at these densities, are all of the same (even) parity and are able to radiate only forbidden lines. The situation dramatically changes near density 10^6 cm^{-3}: the infrared lines become *relatively* weak since the upper levels are collisionally saturated, while the UV lines become stronger because, at this density, levels of odd parity (number 64 and higher) are populated enough by collisions to produce the permitted lines. At higher densities, the permitted UV lines dominate the spectrum.

3. [Fe II] LINES IN THE ORION NEBULA

3.1. *Line List*

We use new observations of the Orion Nebula, made at a point 37″ west of θ^1 Ori C using the Cassegrain echelle spectrograph on CTIO's 4 m Blanco Telescope. Separate spectra were taken in the red and blue spectral regions. The resolution was 10 km s^{-1}. Exposure times of approximately 1 hr in each wavelength region allowed us to measure emission lines down to a limit about 10^4 times weaker than Hβ. Full details of the observation and reduction procedure are given by Baldwin et al. (2000).

Using our model calculations, we compiled a list of [Fe II] lines that can be expected from the Orion Nebula down to the flux limit of our data. Based on this list, we identified 40 distinct forbidden lines of Fe II. Seven of these lines are observed in both blue and red spectra. Table 1 contains [Fe II] data in eight columns:

1. Observed wavelength in the Orion rest frame, defined by H and He lines, in Å;
2. Laboratory wavelength, in Å;
3. "?" for lines with low signal-to-noise ratio ($3.5 < S/N < 7$);
4. Measured velocity, in km s^{-1}, relative to the Orion rest frame;
5. FWHM, in km s^{-1};
6. Reddening-corrected line intensity relative to the intensity of He I λ6678;
7. Signal-to-noise ratio;
8. Notes.

The FWHM is the measured value, which is not corrected for instrumental broadening. The instrumental broadening varies a bit across the CCD but is in the range 8–10 km s^{-1}. The night-sky lines therefore have these widths.

The extinction corrections are differential, zero at 6678 Å and of opposite signs on either side of this wavelength. The amount of extinction corresponds to $E_{B-V} = 0.249$ and has a wavelength dependence as given by Cardelli, Clayton, & Mathis (1989) for $R_V = 5.5$; this prescription is appropriate for correcting the H I and He I lines at this position in the nebula (Baldwin et al. 1991; Baldwin et al. 2000).

All [Fe II] lines are within the velocity range 13 ± 8 km s^{-1}. All the observed lines are produced by transitions within the first 43 levels (see Table 1 and Fig. 3). In some multiplets, we see up to seven lines. Within all the multiplets, the strongest lines predicted by the model have been observed.

3.2. *Comparison with Model Predictions*

The new observations allow us to check our theoretical models. Table 2 shows the spectroscopic data for the observed [Fe II] lines in the blue and red spectra, observed line ratios relative to the intensity He I λ6678 line from both spectra, and predictions from our models. The table contains data in 14 columns:

1. Fe II laboratory air wavelength, in Å;
2. Moore multiplet nomenclature;
3. Multiplet identification;
4. Order number of lower level;
5. Order number of upper level;
6. Energy of lower level, in cm^{-1};
7. Energy of upper level, cm^{-1};
8. Statistical weight of lower level;
9. Statistical weight of upper level;
10. Transition probability, in s^{-1} (Quinet, Le Dourneuf, & Zeippen 1996);

TABLE 1

OBSERVED [Fe II] EMISSION LINES (REDDENING CORRECTED)

Rest Frame Wavelength (Å) (1)	ID Wavelength (Å) (2)	ID? (3)	δV (km s^{-1}) (4)	FWHM (km s^{-1}) (5)	I/6678 (6)	S/N (7)	Notes (8)
4114.566	4114.470	?	7.0	20	0.0025	6.6	Strongest line in multiplet
4177.405	4177.196	?	15.0	16	0.0026	5.6	
4179.218	4178.958	?	18.7	5	0.0010	4.7	
4211.289	4211.099	?	13.5	8	0.0008	4.4	
4244.145	4243.969		12.4	17	0.0118	37.6	
4276.987	4276.829		11.1	20	0.0092	18.1	Possible blend with O II 4276.749 recombination line
4287.587	4287.394		13.5	12	0.0232	64.0	Possible blend with O II 4287.727 recombination line
4352.951	4352.778		11.9	19	0.0051	10.6	
4359.528	4359.333		13.4	13	0.0160	18.6	
4413.984	4413.781		13.8	11	0.0116	63.2	
4416.459	4416.266		13.1	15	0.0141	64.6	
4452.304	4452.098		13.9	13	0.009	33.5	Possible overlap with O II 4452.378
4458.148	4457.945		13.6	17	0.0049	15.7	
4475.104	4474.904		13.4	14	0.0035	16.1	
4492.831	4492.634	?	13.2	11	0.0014	7.8	After subtracting ghost
4515.027	4514.900	?	8.5	16	0.0013	4	From multiplet with 11 lines, strongest at 4416.27
4728.294	4728.068	?	14.3	14	0.0016	7.0	
4774.942	4774.718		14.1	13	0.0017	8.3	Possible line from multiplet with strongest line at 4889.63
4814.741	4814.534		12.9	18	0.0120	28.5	
4889.833	4889.617		13.3	13	0.0067	29.4	Average; from multiplet with strongest line at 4814.55
4905.555	4905.339	?	13.2	12	0.0023	6.7	But possibly [Fe II] 4889.70 from a different multiplet
4947.557	4947.373		11.2	16	0.0049	22.1	
4951.038	4950.744		17.8	34	0.0035	8.4	
4973.653	4973.388	?	16.0	20	0.0036	3.5	
5111.854	5111.627		13.3	12	0.0038	27.5	
5158.951	5158.777		10.1	21	0.0182	56.7	B
5158.956	5158.777		10.4	21	0.0147	56.6	R
5220.275	5220.060	?	12.4	19	0.0014	5.5	R
5220.297	5220.059		13.7	20	0.0015	9.9	B
5261.854	5261.621		13.3	15	0.0136	38.2	B
5261.856	5261.621		13.4	13	0.0112	71.3	R
5269.228	5268.874	?	20.2	20	0.0009	4.1	R Not seen in blue spectrum
5273.577	5273.346		13.2	16	0.0073	35.3	R Average
5273.598	5273.346		14.3	16	0.0067	26.4	B Possible contribution from Ca I 5261.704 ^3D–^3P
5297.037	5296.829	?	11.8	15	0.0008	4.7	R Not seen in blue spectrum
5333.862	5333.646		12.2	17	0.0035	20.9	B
5333.866	5333.646		12.4	18	0.0031	16.5	R
5376.606	5376.452		8.6	40	0.0046	8.4	B
5376.646	5376.452		10.8	23	0.0029	12.1	R Average; fuzzy on two-dimensional image; second strong line in multiplet 5261.61
5433.365	5433.129		13.0	15	0.0022	7.6	R Average; same multiplet as 5273, 5269
5433.369	5433.129		13.3	20	0.0021	10.1	B Cannot tell if real; from same multiplet as 5273, 5269
5747.190	5746.966	?	11.7	17	0.0008	5.5	B
6440.522	6440.400	?	5.7	19	0.0005	4.6	
7155.366	7155.16		8.6	19	0.0150	76.4	
7172.218	7172.00	?	9.1	13	0.0035	6.5	Average
7388.397	7388.18		8.8	20	0.0024	11.2	Flux uncertain; cut by atmospheric absorption
7452.782	7452.54		9.7	19	0.0045	39.2	

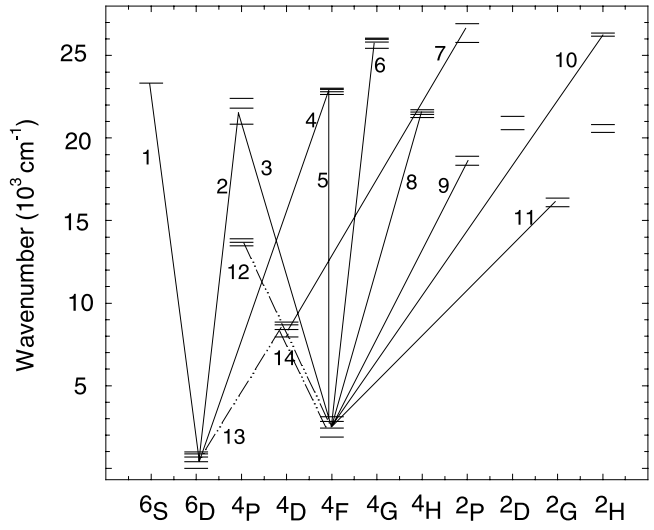

FIG. 3.—Lowest 43 levels of Fe II and the observed multiplets in the Orion Nebula. For simplicity, the diagram does not show all observed lines. The numbers in the diagram correspond to the Moore classification of multiplets shown here in parentheses, which contain multiple lines (in Å): 1 (7F)—4287, 4359, 4414, 4452, 4475; 2 (4F)—4728, 4889; 3 (18F)—5269, 5273, 5433; 4 (6F)—4416, 4458, 4493, 4515; 5 (20F)—4775, 4815, 4905, 4947, 4951, 4973; 6 (21F)—4177, 4244, 4277, 4353; 7 (34F)—5747; 8 (19F)—5112, 5159, 5220, 5262, 5297, 5334, 5376; 9 (none)—6440; 10 (23F)—4114, 4179, 4211; 11 (14F)—7155, 7172, 7388, 7453; 12 (13F), 13 (none), and 14 (none). Multiplets 13 and 14 are in the near-infrared (not covered by the current observations).

11. Reddening-corrected line intensity from the blue spectrum, relative to He I λ6678;

12. Reddening-corrected line intensity from the red spectrum, relative to He I λ6678;

13. Predictions from the pumping model (model C, after Baldwin et al. 1996);

14. Predictions from the collisional model (model II, after Baldwin et al. 1996).

Figure 4 compares intensities of observed [Fe II] lines with the theoretical intensities calculated both in the pure collisional model (model II, Baldwin et al. 1996) and with pumping in the framework provided by model C (Baldwin et al. 1996). Model II is a simple limit of our Fe II model (one zone, constant temperature, constant density, no continuum radiation flux, no line pumping, no interactions with other species) and corresponds to the Bautista et al. (1994) and Bautista, Peng, & Pradhan (1996) collisional model with density of $n_e = 10^4$ cm^{-3}. Model C is calculated with the parameters taken from Baldwin et al. (1991) with improved gas-phase elemental abundances based on results from Osterbrock et al. (1992) and Rubin et al. (1991, 1992): H : He : C : N : O : Ne : Na : Mg : Al : Si : S : Cl : Ar : Ca : Fe = $1 : 0.095 : 3 \times 10^{-4} : 7 \times 10^{-5} : 4 \times 10^{-4} : 6 \times 10^{-5} : 3 \times 10^{-7} : 3 \times 10^{-6} : 2 \times 10^{-7} : 4 \times 10^{-6} : 10^{-5} : 10^{-7} : 3 \times 10^{-6} : 2 \times 10^{-8} : 3 \times 10^{-6}$, grains and ionization by the incident continua from the four Trapezium stars are included.

Clearly, the pure collisional model significantly underpredicts the intensities. There is a trend toward greater underprediction with decreasing wavelength, in the same sense as would be caused by too small a reddening correction. Over the total wavelength interval covered by the [Fe II] lines, the data have already been corrected differentially by 0.67 mag (a factor 1.86). The correction required to offset the trend toward underprediction would be a *further* differential factor of about 4, much too large to be attributed to an incorrect reddening correction. The explanation is that lines with shorter wavelengths tend to arise from upper levels with higher energies. These higher levels are harder to excite by collisions alone, so the lines are systematically underpredicted (a plot of the theoretical to observed ratio vs. energy of the upper level shows this clearly). We conclude that density (collisional excitation) is not the only factor determining the population of the upper levels.

Figure 5 plots the predicted intensities of model C versus the observed ones. No correlation of the deviations with line intensity is found.

Figure 6 presents the ratios of the predicted to observed intensities in this model with pumping, plotted against the energies of upper levels of the transitions. There is only a slight trend in that the higher levels tend to be more underpopulated in the model. This is because the level populations depend on the details of the pumping lines and the

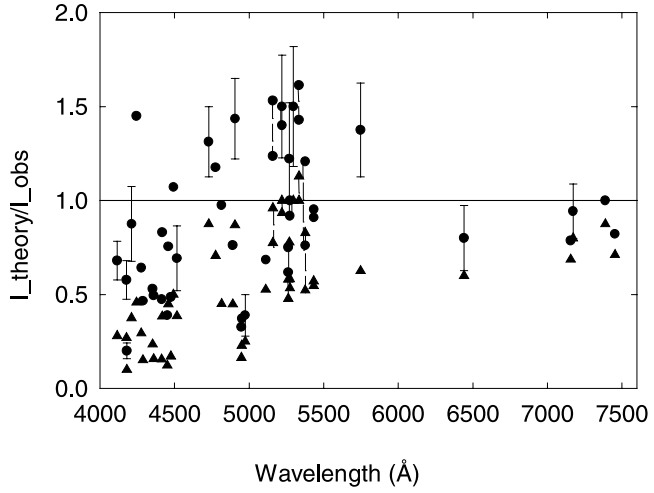

FIG. 4.—Ratio of the predicted intensities of [Fe II] lines to the observed values for model C (with pumping, *circles*) and model II (no pumping, *triangles*). Data for lines observed in both blue and red spectra are joined with a dashed bar. Error bars are shown for lines with S/N < 7.

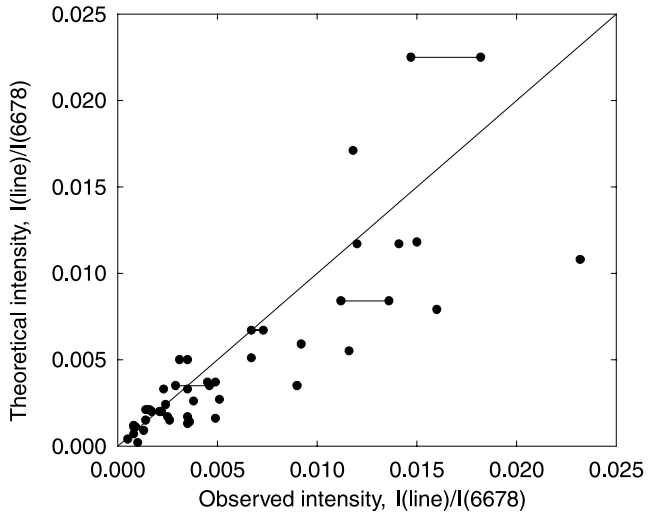

FIG. 5.—Predicted intensities vs. the observed intensities of [Fe II] lines, model C. Data for lines observed in both blue and red spectra are joined with a bar.

TABLE 2

OBSERVED AND PREDICTED [Fe II] LINE INTENSITIES

ID WAVELENGTH (Å) (1)	MOORE (2)	MULTIPLET (3)	ORDER Lower (4)	ORDER Upper (5)	E_l (cm^{-1}) (6)	E_u (cm^{-1}) (7)	g_l (8)	g_u (9)	A_{ul} (s^{-1}) (10)	INTENSITY/I(6678) Blue (11)	Red (12)	Pumping (13)	Collisional (14)
4114.470	23F	a^4F–b^2H	6	42	1873	26170	10	12	0.103	0.0025	...	0.0017	0.0007
4177.196	21F	a^4F–a^4G	6	39	1873	25805	10	10	0.194	0.0026	...	0.0015	0.0007
4178.958	23F	a^4F–b^2H	7	43	2430	26353	8	10	0.016	0.0010	...	0.0002	0.0001
4211.099	23F	a^4F–b^2H	7	42	2430	26170	8	12	0.044	0.0008	...	0.0007	0.0003
4243.969	21F	a^4F–a^4G	6	37	1873	25429	10	12	1.12	0.0118	...	0.0171	0.0054
4276.829	21F	a^4F–a^4G	7	39	2430	25805	8	10	0.819	0.0092	...	0.0059	0.0027
4287.394	7F	a^6D–a^6S	1	36	0	23318	10	6	1.65	0.0232	...	0.0108	0.0035
4352.778	21F	a^4F–a^4G	8	39	2838	25805	6	10	0.380	0.0051	...	0.0027	0.0012
4359.333	7F	a^6D–a^6S	2	36	385	23318	8	6	1.220	0.0160	...	0.0079	0.0025
4413.781	7F	a^6D–a^6S	3	36	668	23318	6	6	0.858	0.0116	...	0.0055	0.0018
4416.266	6F	a^6D–b^4F	1	32	0	22637	10	10	0.454	0.0141	...	0.0117	0.0054
4452.098	7F	a^6D–a^6S	4	36	863	23318	4	6	0.548	0.009	...	0.0035	0.0011
4457.945	6F	a^6D–b^4F	2	33	385	22810	8	8	0.279	0.0049	...	0.0037	0.0022
4474.904	7F	a^6D–a^6S	5	36	977	23318	2	6	0.267	0.0035	...	0.0017	0.0006
4492.634	6F	a^6D–b^4F	2	32	385	22637	8	10	0.060	0.0014	...	0.0015	0.0007
4514.900	6F	a^6D–b^4F	3	33	668	22810	6	8	0.065	0.0013	...	0.0009	0.0005
4728.068	4F	a^6D–b^4P	3	30	668	21812	6	4	0.478	0.0016	...	0.0021	0.0014
4774.718	20F	a^4F–b^4F	6	33	1873	22810	10	8	0.163	0.0017	...	0.0020	0.0012
4814.534	20F	a^4F–b^4F	6	32	1873	22637	10	10	0.521	0.0120	...	0.0117	0.0054
4889.617	4F	a^6D–b^4P	2	24	385	20831	8	6	0.347	0.0067	...	0.0051	0.0030
4905.339	20F	a^4F–b^4F	7	33	2430	22810	8	8	0.285	0.0023	...	0.0033	0.0020
4947.373	20F	a^4F–b^4F	7	32	2430	22637	8	10	0.075	0.0049	...	0.0016	0.0008
4950.744	20F	a^4F–b^4F	8	35	2838	23031	6	4	0.225	0.0035	...	0.0013	0.0008
4973.388	20F	a^4F–b^4F	8	34	2838	22939	6	6	0.183	0.0036	...	0.0014	0.0009
5111.627	19F	a^4F–a^4H	6	27	1873	21430	10	12	0.131	0.0038	...	0.0026	0.0020
5158.777	19F	a^4F–a^4H	6	25	1873	21252	10	14	0.605	0.0182	0.0147	0.0225	0.0141
5220.060	19F	a^4F–a^4H	7	28	2430	21582	8	10	0.144	0.0015	0.0014	0.0021	0.0014
5261.621	19F	a^4F–a^4H	7	27	2430	21430	8	12	0.429	0.0136	0.0112	0.0084	0.0065
5268.874	18F	a^4F–b^4P	8	30	2838	21812	6	4	0.288	...	0.0009	0.0011	0.0007
5273.346	18F	a^4F–b^4P	6	24	1873	20831	10	6	0.550	0.0067	0.0073	0.0067	0.0039
5296.829	19F	a^4F–a^4H	8	29	2838	21712	6	8	0.118	...	0.0008	0.0012	0.0008
5333.646	19F	a^4F–a^4H	8	28	2838	21582	6	10	0.351	0.0035	0.0031	0.0050	0.0035
5376.452	19F	a^4F–a^4H	9	29	3117	21712	4	8	0.348	0.0046	0.0029	0.0035	0.0024
5433.129	18F	a^4F–b^4P	7	24	2430	20831	8	6	0.174	0.0021	0.0022	0.0020	0.0012
5746.966	34F	a^4D–b^2P	11	38	8392	25788	6	4	0.373	0.0008	...	0.0011	0.0005
6440.400	...	a^4F–a^2P	8	19	2838	18361	6	4	0.0213	...	0.0005	0.0004	0.0003
7155.16.....	14F	a^4F–a^2G	6	17	1873	15845	10	10	0.153	...	0.0150	0.0118	0.0103
7172.00.....	14F	a^4F–a^2G	7	18	2430	16369	8	8	0.0588	...	0.0035	0.0033	0.0028
7388.18.....	14F	a^4F–a^2G	8	18	2838	16369	6	8	0.0448	...	0.0024	0.0024	0.0021
7452.54.....	14F	a^4F–a^2G	7	17	2430	15845	8	10	0.0492	...	0.0045	0.0037	0.0032

subsequent radiative cascade (to be discussed) and not simply on the energy above the ground state. In the model with pumping, the predicted intensities are generally within $\pm 50\%$ of the observed ones. The overall agreement is judged to be consistent with the uncertainties in the observations, the dereddening corrections, and the quality of the atomic data. Note that lines at 4277, 4287, and 4452 Å are included in the comparison, even though their observed intensities might be enhanced by the contribution of the O II recombination lines; since they are underpredicted by both models, the contamination cannot be large.

Note that we did not try to fit the new observations: we simply used the same parameters as found by Baldwin et al. (1996) in the models. For the model with pumping, the general agreement of the predicted and observed [Fe II] line spectrum is quite satisfactory. We checked that there are no strong theoretical lines predicted in model C that have not been observed. There are no major systematic discrepancies between the modeled and observed line intensities. If anything, the lines are slightly underpredicted, so that the gas phase Fe/H abundance ought to be adjusted to 4×10^{-6} from 3×10^{-6} as used in model C.

We have identified pumping routes that are important in exciting the observed [Fe II] lines. The full pumping scheme is summarized in Figure 7. The ground term (a^6D) and the lowest excited term (a^4F) are populated by collisions at densities above 10^4 cm^{-3}. Although the populations of the first five levels within the ground term are higher than the population of the sixth level, pumping from them does not produce optical forbidden lines. Electrons excited from the first five levels by UV radiation decay back to the ground term since the branching ratios are strongly dominated by the resonant transitions. The main pumping routes start from the sixth level, the lowest in a^4F, $g = 10$ at 1873 cm^{-1} (see detail in Fig. 3) since a considerable part of the electrons excited from the sixth level then cascade down through the intermediate levels, emitting the forbidden optical lines. In detail, radiative pumping excites electrons

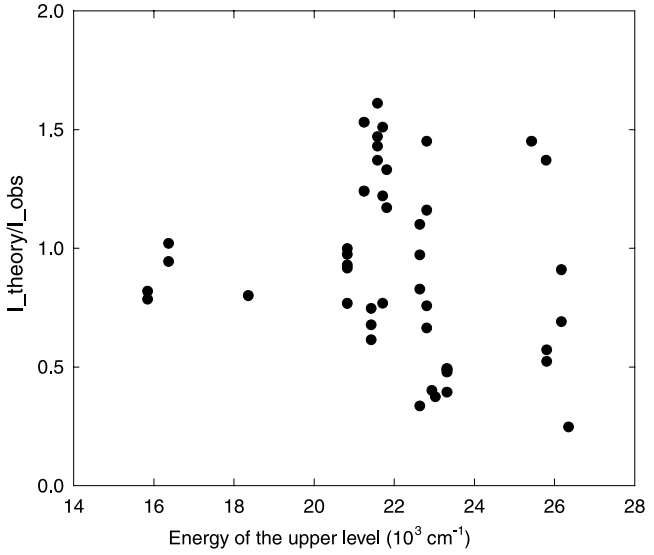

FIG. 6.—Ratio of the predicted intensities of [Fe II] lines (model C) to the observed values vs. the energy of upper levels of the transitions.

from this level to levels 122 ($z\,^4G^o$, $g = 12$), 137 ($y\,^4D^o$, $g = 8$), and 172 ($x\,^4F^o$, $g = 10$). Branching ratios of transitions down from these levels are favorable for populating levels 25 ($a\,^4H$, $g = 14$), 32 ($b\,^4F$, $g = 10$), 24 ($b\,^4P$, $g = 6$), and 37 ($a\,^4G$, $g = 12$). In turn, these are the upper levels of many of the [Fe II] lines observed in the Orion Nebula, including the strongest lines in the relevant multiplets ($\lambda\lambda$5433, 5273, 5159, 4947, 4890, 4814, 4492, 4416, 4244). Pumping from levels higher than the sixth level is less efficient since they are less populated by collisions and so have smaller populations.

Figures 8, 9, 10, and 11 present comparisons for the strong multiplets in the same format as Figure 4. In the strongest multiplet, $a\,^4F$–$a\,^4H$ (19 F), seven lines have been identified, and five from them have been observed in both the red and blue spectra (as shown by the pairs of points). The $a\,^4F$–$a\,^2G$ (21 F) and $a\,^6D$–$b\,^4F$ (6 F) multiplets have four observed lines each. Note that all the theoretically strongest lines in these multiplets have been observed. The

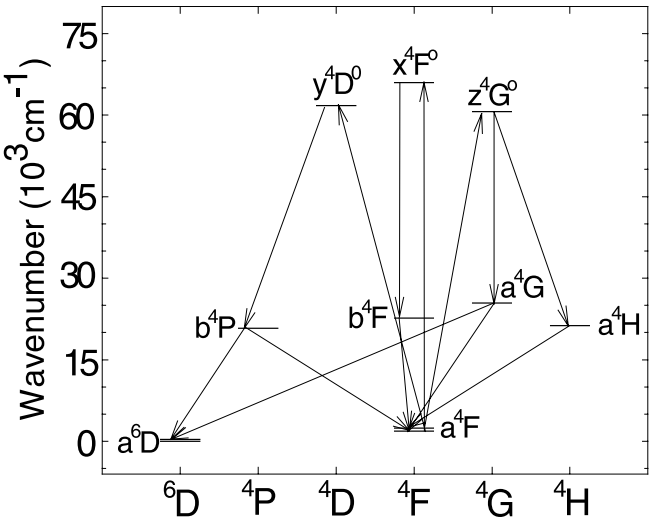

FIG. 7.—Pumping scheme showing the main routes starting from level 6 ($a\,^4F$ at 1873 cm^{-1}), which can be excited up to level 172 at 66013 cm^{-1}. Cascades down produce the observed [Fe II] optical lines.

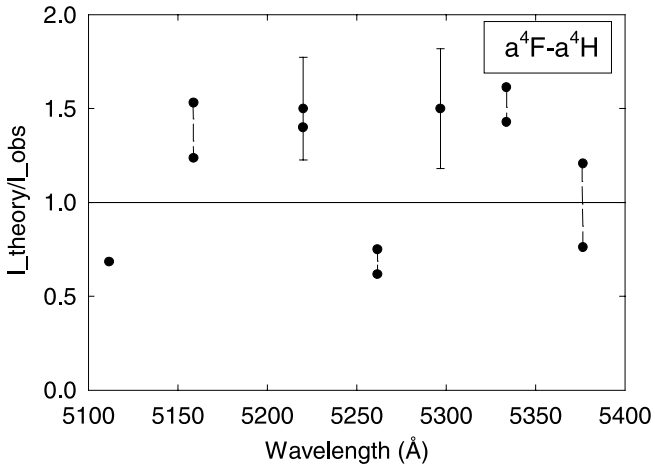

FIG. 8.—Ratio of the predicted intensities (model C) to the observed values for the [Fe II] $a\,^4F$–$a\,^4H$ multiplet (19F). Data for lines observed in both blue and red spectra are joined with a dashed bar. Error bars are shown for lines with S/N < 7.

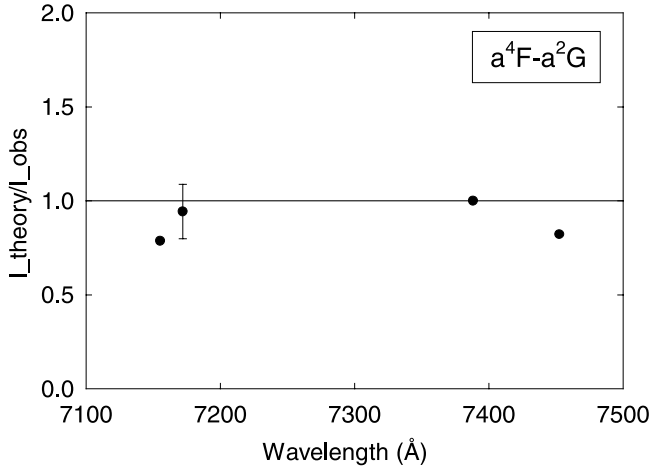

FIG. 9.—Same as Fig. 7 for the $a\,^4F$–$a\,^2G$ multiplet (14F)

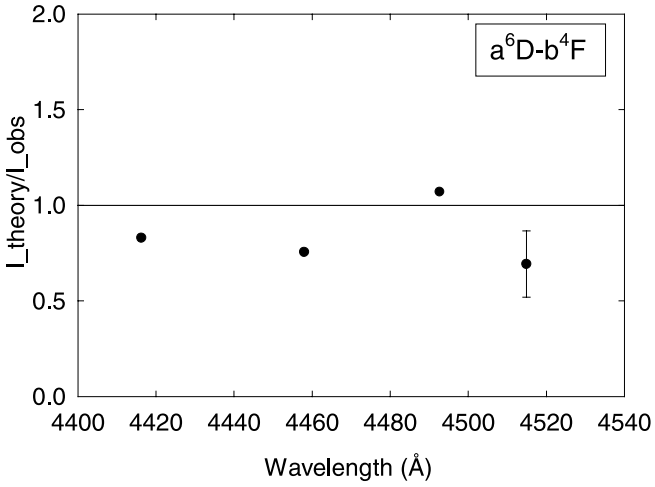

FIG. 10.—Same as Fig. 7 for the $a\,^6D$–$b\,^4F$ multiplet (6F)

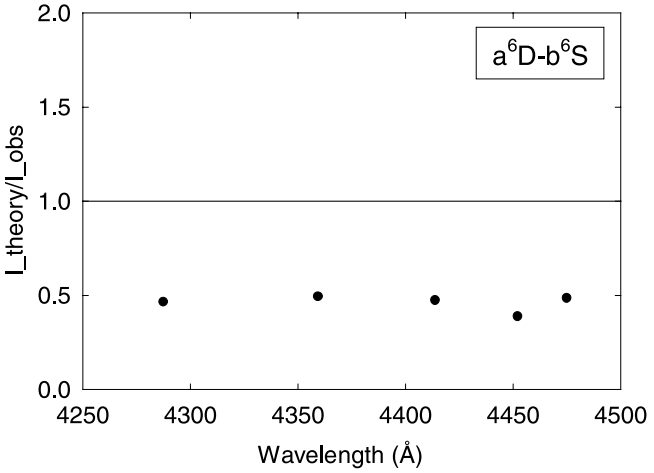

FIG. 11.—Same as Fig. 7 for the $a\,^6D$–$a\,^6S$ multiplet (7F, single upper level).

theoretical intensities of all five lines from the $a\,^6D$–$a\,^6S$ (7 F) multiplet (single upper level) are 50% weaker than the observed ones (see Fig. 11). Obviously, there is a missed excitation mechanism for the $a\,^6S$ level or the collisional data are wrong for this level.

4. SUMMARY

Our previous model of [Fe II] emission (Baldwin et al. 1996) included collisional and continuum pumping processes and had certain difficulties in reproducing the observed [Fe II] line ratios. In particular, the theoretical lines at 4277, 5262, and 5334 Å were three to four times too weak compared with their observed intensities. However, that comparison was made on a basis of very few [Fe II] lines and different observations, with different uncertainties in intensity measurements. Two main advances have been made. First, the calculations depend on the accuracy of the atomic data. New collision data for transitions between the lowest levels were added. Second, the comparisons presented in this paper are based on our new set of observations, which includes many new lines. Our theoretical model of Fe II emission now is in good agreement with the new observational data, including the lines mentioned above, and there is no need to add a physically distinct emission-line region to Orion to explain the data. Within this model, the gas phase Fe/H is 4×10^{-6}.

The comparison between the predicted and the observed data confirms the importance of radiative pumping fluorescence processes for the formation of the [Fe II] emission spectra. The main lesson here is that optical [Fe II] lines cannot be used for straightforward density diagnostics in H II regions.

Research in Nebula Astrophysics at the University of Kentucky is supported by NSF through AST 96-17083 and by STScI through AR 08387. Research by P. G. M. is supported by National Science and Engineering Research Council of Canada. We are grateful to M. Bautista for sending us the Fe II collision strengths in numerical form.

REFERENCES

Baldwin, J. A., et al. 1991, ApJ, 374, 580
Baldwin, J. A., et al. 1996, ApJ, 468, L115
Baldwin, J. A., Verner, E. M., Verner, D. A., Ferland, G. J., Martin, P. G., Korista, K. T., & Rubin, R. H. 2000, ApJS, 129, 1
Bautista, M. A., Peng, J., & Pradhan, A. K. 1996, ApJ, 460, 372
Bautista, M. A., Pradhan, A. K., & Osterbrock, D. E. 1994, ApJ, 432, L135
Cardelli, J. A., Clayton, G. C., & Mathis, J. S. 1989, ApJ, 345, 245
Esteban, C., Peimbert, M., Torres-Peimbert, S., & Escalante, V. 1998, MNRAS, 295, 401
Ferland, G. J., Korista, K. T., Verner, D. A., Ferguson, J. W., Kingdon, J. B., & Verner, E. M. 1998, PASP, 110, 761
Johansson, S. 1978, Phys. Scr., 18, 217
Lucy, L. 1995, A&A, 294, 555
Osterbrock, D. E. 1989, Astrophysics of Gaseous Nebulae and Active Galactic Nuclei (Mill Valley: University Science Books)
Osterbrock, D. E., Tran, H. D., & Veilleux, S. 1992, ApJ, 389, 305
Quinet, P., Le Dourneuf, M., & Zeippen, C. J. 1996, A&AS, 120, 361
Rodriguez, M. 1999, A&A, 348, 222
Rubin, R. H., Erickson, E. F., Haas, M. R., Colgan, S. W. J., Simpson, J. P., & Defour, R. J. 1992, in IAU Symp. 150, The Astrochemistry of Cosmic Phenomena, ed. P. D. Singh (Dordrecht: Kluwer), 281
Rubin, R. H., Simpson, J. P., Haas, M. R., & Erickson, E. F. 1991, ApJ, 374, 564
Verner, E. M., Verner, D. A., Korista, K. T., Ferguson, J. W., Hamann, F., & Ferland, G. J. 1999, ApJS, 120, 101